Letters

A Reconfigurable Rectifier-Based Power Improving Method of Free-Standing Two-Coil Magnetic Field Energy Harvesters Over a Wide Load Range

Yong Li, *Senior Member, IEEE*, Yihua Yan, Huanyu Yang, Jiefeng Hu, *Senior Member, IEEE*, and Zhengyou He, *Senior Member, IEEE*

***Abstract*—Free-standing magnetic field energy harvesters (FSMFEHs) have promising potential in charging sensors used in electrical power grids. The output power of the FSMFEH is highly dependent on the load resistance. However, the load resistance of the sensors varies over a wide range during the operation process. Therefore, a crucial challenge for an FSMFEH system is to maintain high output power over a wide load range. In this letter, an innovative reconfigurable rectifier-based FSMFEH system with two coils connected in parallel is proposed. First, a new structure of two identical coils in parallel is proposed in magnetic energy harvesting applications. Then, a reconfigurable rectifier with two operation modes is developed to incorporate the new coil structure. By switching between the full-bridge mode and the half-bridge mode according to the actual load demand, the proposed FSMFEH can maintain high output power over a wide load range. In addition, the mode transition can be easily achieved by shorting one of the diodes, leading to a simple and low-loss control. The effectiveness of the proposed FSMFEH system is verified based on a laboratory prototype. It is provided that the experimental result is consistent with the theoretical analysis. The output power can be maintained above 8.19 mW within the 50–1500 Ω range when the busbar current is 100 A.**

***Index Terms*—Free-standing magnetic field energy harvester (FSMFEH), power improving, two-coil system, wide load range.**

Manuscript received 7 October 2022; revised 23 November 2022 and 25 December 2022; accepted 17 January 2023. Date of publication 23 January 2023; date of current version 10 March 2023. This work is supported in part by Young Elite Scientist Sponsorship Program by China Association for Science and Technology, in part by the Star of Science and Technology in Southwest Jiaotong University under Grant 2682021CG018, in part by Young Eagle Program in Southwest Jiaotong University, in part by the Chengdu Guojia Electrical Engineering Company, Ltd. under Grant NEEC-2022-A07, in part by the Cutting-edge Science and Technology Cultivation Project of Southwest Jiaotong University under Grant 2682022KJ005, and in part by the Sichuan Science and Technology Innovation Programme under Grant 2022017. *(Corresponding author: Yong Li.)*

Yong Li, Yihua Yan, Huanyu Yang, and Zhengyou He are with the National Rail Transit Electrification and Automation Engineering Technique Research Center, Southwest Jiaotong University, Chengdu 610031, China, and also with the School of Electrical Engineering, Southwest Jiaotong University, Chengdu 610031, China (e-mail: leeo1864@163.com; yyh1@my.swjtu.edu.cn; 983911020@qq.com; hezy@swjtu.edu.cn).

Jiefeng Hu is with the Institute of Innovation, Science and Sustainability, Federation University Australia, Mount Helen, VIC 3353, Australia, and also with the Centre for New Energy Transition Research, Federation University Australia, Mount Helen, VIC 3353, Australia (e-mail: j.hu@federation.edu.au).

Color versions of one or more figures in this article are available at https://doi.org/10.1109/TPEL.2023.3238763.

Digital Object Identifier 10.1109/TPEL.2023.3238763

I. Introduction

BUSBARS in switchgears play a crucial role in transmitting electrical energy. To ensure a safe and stable operation of the busbars, wireless sensors are used to monitor essential information on the busbars, e.g., temperature, voltage, current, humidity, etc. However, the limited life span of batteries that power the wireless sensors becomes a bottleneck because it increases the cost to replace them frequently [1]. Therefore, it is necessary to develop a reliable and stable power supply method to achieve a self-sustainable monitoring system [2].

Energy harvesting (EH) technologies can harvest energy from the ambient environment, such as solar, wind, vibration, radio frequency, magnetic field, etc. Solar EH technology is relatively mature and has been extensively researched to date. However, solar energy is affected by weather conditions, which cannot be applied to the busbar of switchgear [3]. Similar situations exist in wind EH technology [4]. Vibration and radio frequency energy harvesters are not limited by weather conditions, but they produce extremely low power densities. At present, the power densities of the vibration and radio frequency energy harvesters are μW/cm^3 level. For example, the harvesters developed in references [5] and [6] can harvest an output power of 143.6 and 21.4 μW, respectively.

The magnetic field energy harvester (MFEH) harvests energy from the magnetic field around the busbars [7], [8], [9], [10], [11], [12], [13]. Unlike solar and wind EH technology, MFEH is independent of weather conditions [7], [8]. In addition, it has a higher power density than vibration and radio frequency energy harvesters [7], [8], [9], [10], [11], [12], [13]. Therefore, MFEH is suitable for harvesting energy near busbars [13].

MFEH can be classified into two types [7], [8], [9], [10], [11], [12], [13]. The first type is called cable-clamped MFEH (CCMFEH) [7], [8], and its power density is relatively high. However, the core diameter of the CCMFEH will increase with increasing busbar width, which makes the CCMFEH system not universal. The second type is the free-standing MFEH (FSMFEH) [10], [11], [12], [13], which can be placed anywhere on the busbar with an alternating magnetic field and can overcome the disadvantage mentioned above. For FSMFEHs, the latest research result shows that a power density of 4.182 mW/cm^3 can be achieved [13]. Despite the above advantages, there is still

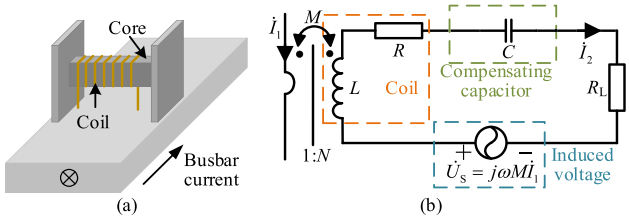

Fig. 1. Conventional FSMFEH system. (a) System placed on the busbar. (b) Equivalent circuit.

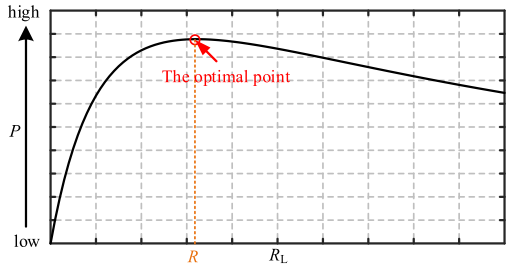

Fig. 2. Curve of the output power P against the equivalent AC load R_L.

a critical problem that need to be addressed for the FSMFEH. The characteristic of output power against load changes is further analyzed in [12] and [13]. It is found that when the load resistance of the sensor decreases from the optimal load, the output power generated from the FSMFEH will fall rapidly below the maximum power point. In this case, the stable operation of a sensor will be adversely influenced due to the low power supply. This is the key challenge faced by FSMFEH systems for charging wireless sensors in electrical power grids [14].

Currently, there are two main ways to improve the power transfer capability of FSMFEHs to tackle the issue of variable load. The first way is to improve the power by increasing the size of the core [10], [12]. For example, in [12], the output power of the FSMFEHs can achive from 40 to 200 mW over the 10–200 Ω load range. However, the size of the core is 24.2 cm × 10 cm × 10 cm, which means that the cost of the core is very high. Meanwhile, due to the limitation of installation space in the busbar environment, such a large core cannot be applied in the busbar environment. The second way is to improve the output power of the system by designing the core structure, such as a helical core [11]. As the length of the core is increased, the output power of the system is significantly improved. However, such a helical core is complicated and expensive to make.

In light of this, a reconfigurable rectifier-based FSMFEH system with two coils connected in parallel is proposed in this letter. To the best of our knowledge, this method has never been done for the FSMFEH before. The proposed system only needs to drive a switch, and thus, it has simple control and low power loss. Compared with the existing methods [10], [11], [12], the method proposed in this letter requires neither increasing the size of the core nor making complex core shapes. Based on the structure of two identical coils in parallel, high output power over a wide range can be harvested by switching the rectifier between full-bridge and half-bridge modes.

The contributions of this letter are listed as follows.

1) A two-coil FSMFEH system with a reconfigurable rectifier is proposed in this letter, which can work in two operating modes: the full-bridge rectifier mode and the half-bridge rectifier mode. Besides, the mathematical models between the equivalent load and the output power of the two modes are derived.
2) Based on the above mathematical models, the relationship between the optimal dc load of the two modes is obtained, i.e., the optimal dc load of the half-bridge mode is four times of the full-bridge mode. Meanwhile, the theoretical load boundary between the two modes is derived. Then, the operating mode of the system can be selected according to the relationship between the actual load and the theoretical boundary load. The proposed system can maintain high output power over a wide load range by selecting work in the full-bridge mode or the half-bridge mode. The experimental results show that the output power can be maintained above 8.19 mW within the 50–1500 Ω range when the busbar current is 100 A.

II. Conventional Energy Harvester

Fig. 1(a) shows the conventional FSMFEH system placed on the busbar. The equivalent circuit of the FSMFEH system is shown in Fig. 1(b). $\dot{I}_1$ is the busbar current. M is the mutual inductance between the busbar and the harvesting coil. L is the self-inductance of the coil, and R is the coil resistance. C is the compensating capacitor, which is added in series to the circuit to eliminate the reactive power generated by the self-inductance L of the coil, thus, $C = 1/(\omega^2 L)$. N is the number of coil winding turns. R_L is the equivalent ac load resistance. According to Faraday's law, the induced coil voltage $\dot{U}_S$ can be expressed as

$$\dot{U}_{\mathrm{S}} = j\omega M\dot{I}_1. \tag{1}$$

The harvested power delivered to the load can be calculated as

$$P = \frac{U_S^2}{(R_L + R)^2} R_L = \frac{\omega^2 I_1^2 R_{\mathrm{V}} M^2}{(R_L + R)^2}. \tag{2}$$

According to (2), the curve of the output power P against the equivalent ac load R_L is plotted in Fig. 2. It can be observed that the curve has an optimal point where the output power is maximum. The corresponding optimal equivalent ac load can be solved by setting its derivative to zero as follows:

$$\frac{dP}{dR_L} = 0. \tag{3}$$

Then, the optimal load $R_{L\mathrm{eq}}$ is yielded as

$$R_{L\mathrm{eq}} = R. \tag{4}$$

The maximum output power is

$$P_{\max} = \frac{\omega^2 I_1^2 M^2}{4R}. \tag{5}$$

As shown in Fig. 2, it can be further found that the output power P falls slightly with the increase in R_L when R_L is larger

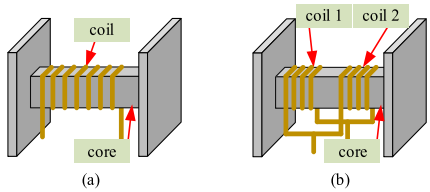

Fig. 3. Harvesting coil structure of the FSMFEH system. (a) Conventional coil structure. (b) Proposed coil structure.

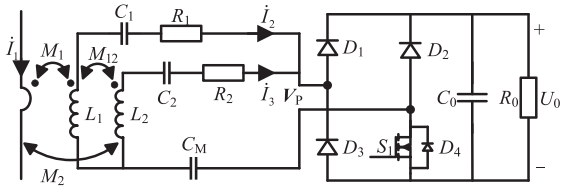

Fig. 4. Reconfigurable rectifier-based FSMFEH system.

than the optimal value. In contrast, P drops rapidly with the decrease in R_L when R_L is smaller than the optimal value. This reveals the difficulty in maintaining high power output for conventional FSMFEH systems under light load conditions. In the following section, a new energy harvester design is proposed to reshape the P-R_L curve. The purpose is to enhance output power, particularly for small loads.

III. New Energy Harvester Design

In the new design, the conventional coil is split into two identical small coils connected in parallel, as depicted in Fig. 3. Based on this, the proposed reconfigurable rectifier-based FSMFEH system is illustrated in Fig. 4. In the proposed system, L_1 is the self-inductance of coil 1, and L_2 is the self-inductance of coil 2. R_1 is the coil resistance of coil 1, R_2 is the coil resistance of coil 2. M_1 is the mutual inductance between the busbar and coil 1. M_2 is the mutual inductance between the busbar and coil 2. M_{12} is the mutual inductance between coils 1 and 2. Because the two coils are split from the conventional coil, $R_1 = R_2 = R/2$, $M_1 = M_2 = M/2$, $L_1 = L_2$. C_1, C_2, and C_M are compensating capacitors on each branch, respectively. V_P is the phasor of the input voltage v_P of the rectifier. R_0 is the dc load. U_0 is the dc output voltage. The rectifier consists of three diodes and a switch, leading to two models depending on the operation of switch S_1.

A. Mode 1: Full-Bridge Mode

A full-bridge rectifier can be gained when switch S_1 is turned OFF, as shown in Fig. 5(a). The equivalent circuit of this full-bridge rectifier is presented in Fig. 5(b).

R_{FL} is plotted in Fig. 5(b) as an equivalent ac load in full-bridge mode. It can be expressed as [15]

$$R_{FL} = \frac{8}{\pi^2} R_0 = R_L. \tag{6}$$

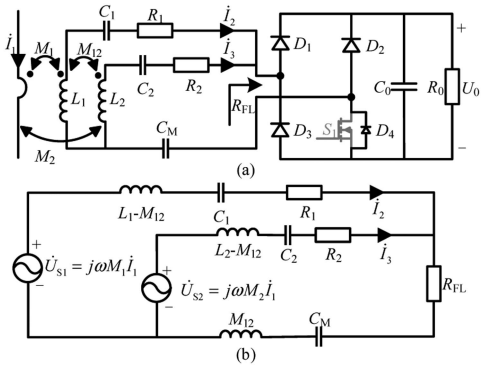

Fig. 5. Proposed FSMFEH system with a full-bridge rectifier. (a) S_1 is turned OFF. (b) Equivalent circuit.

By applying Kirchhoff's voltage law, the equivalent circuit can be described by

$$\begin{cases} j\omega M_1 \dot{I}_1 - Z_1 \dot{I}_2 - Z_M(\dot{I}_2 + \dot{I}_3) - \dot{I}_2 R_1 = (\dot{I}_2 + \dot{I}_3) R_L \\ j\omega M_2 \dot{I}_1 - Z_2 \dot{I}_3 - Z_M(\dot{I}_2 + \dot{I}_3) - \dot{I}_3 R_2 = (\dot{I}_2 + \dot{I}_3) R_L \end{cases} \tag{7}$$

where Z_1, Z_2, and Z_M can be expressed as

$$\begin{cases} Z_1 = j\omega(L_1 - M_{12}) + \frac{1}{j\omega C_1} \\ Z_2 = j\omega(L_2 - M_{12}) + \frac{1}{j\omega C_2} \\ Z_M = j\omega M_{12} + \frac{1}{j\omega C_M} \end{cases} \tag{8}$$

where C_1, C_2, and C_M are compensating capacitors, and they can be expressed as

$$\begin{cases} C_1 = \frac{1}{\omega^2(L_1 - M_{12})} \\ C_2 = \frac{1}{\omega^2(L_2 - M_{12})} \\ C_M = \frac{1}{\omega^2 M_{12}} \end{cases}. \tag{9}$$

Then, the output power can be derived as

$$P_F = \frac{4\omega^2 I_1^2 R_L M^2}{(4R_L + R)^2}. \tag{10}$$

The optimal load R_{FL_opt} for achieving the maximum output power can be obtained by

$$R_{FL\_opt} = \frac{R}{4}. \tag{11}$$

Then, the maximum output power is

$$P_{FMAX} = \frac{\omega^2 I_1^2 M^2}{4R} \tag{12}$$

According to the above analysis and comparing (11) and (12) with (4) and (5), the optimal equivalent load of the full-bridge mode is only a quarter of that in the conventional system, but the maximum output power is maintained. Now, since R_{Lopt} can be reduced by 75%, i.e., R_{Lopt} will move to the left in Fig. 3, higher output power can be achieved in the small-load range.

B. Mode 2: Half-Bridge Mode

By switching on S_1, a half-bridge rectifier can be obtained, as depicted in Fig. 6, where the equivalent ac load can be

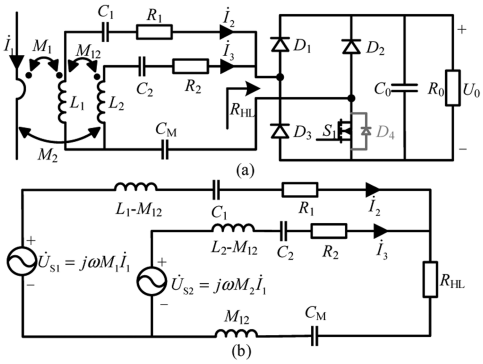

Fig. 6. Proposed FSMFEH system with a half-bridge rectifier. (a) S_1 is turned ON. (b) Equivalent circuit.

expressed as

$$R_{\mathrm{HL}} = \frac{2}{\pi^2} R_0 = \frac{1}{4} R_L. \tag{13}$$

By applying Kirchhoff's voltage law, the equivalent circuit is

$$\begin{cases} j\omega M_1 \dot{I}_1 - Z_1 \dot{I}_2 - Z_M(\dot{I}_2 + \dot{I}_3) - \dot{I}_2 R_1 = (\dot{I}_2 + \dot{I}_3)\frac{R_L}{4} \\ j\omega M_2 \dot{I}_1 - Z_2 \dot{I}_3 - Z_M(\dot{I}_2 + \dot{I}_3) - \dot{I}_3 R_2 = (\dot{I}_2 + \dot{I}_3)\frac{R_L}{4} \end{cases}. \tag{14}$$

According to (8), (9), Z_1, Z_2, and Z_M can be obtained: $Z_1 = 0$; $Z_2 = 0$; and $Z_M = 0$.

Then, the output power can be derived as

$$P_H = \frac{\omega^2 I_1^2 R_L M^2}{(R_L + R)^2}. \tag{15}$$

Accordingly, the optimal load $R_{\mathrm{HL\_opt}}$ can be obtained by

$$R_{\mathrm{HL\_opt}} = R. \tag{16}$$

The maximum output power can be calculated by

$$P_{H\mathrm{MAX}} = \frac{\omega^2 I_1^2 M^2}{4R}. \tag{17}$$

In this case, compared with the conventional system, the optimal load and the maximum output power are not changed, which means that the curves of output power against load changes of the half-bridge mode and the conventional system are overlapped.

C. Switching Boundary Analysis

For a better illustration, the curves of output power against equivalent ac load changes of the full-bridge mode and the half-bridge mode under the same set of system parameters are shown in Fig. 7. R_i is the corresponding load at the intersection of the two curves with the same output power, it can be solved

$$P_F = P_H. \tag{18}$$

Then, the load at the intersection of the two curves R_i is yielded as

$$R_i = \frac{R}{2}. \tag{19}$$

It is worth noting that the R_i here is the equivalent ac load. In this letter, the dc load value of the switching point corresponding

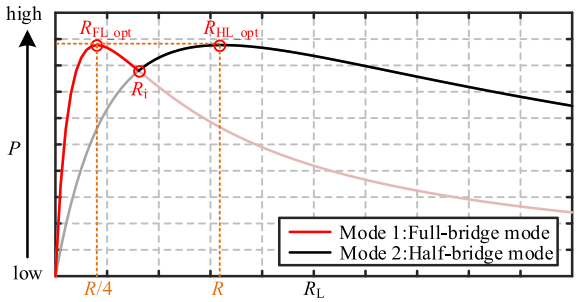

Fig. 7. Theoretical curves that P against R_L under the different modes.

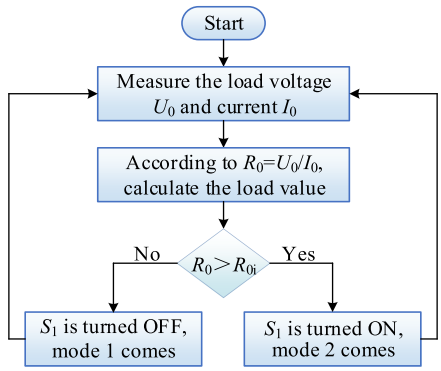

Fig. 8. Switching procedure.

to R_i is defined as R_{0i}. According to (6), the dc load R_{0i} can be expressed as

$$R_{0i} = \frac{\pi^2}{8} R_i = \frac{\pi^2}{16} R. \tag{20}$$

Now, we disclose the most important finding in this research work to guide practical operation. When the dc load of the FSMFEH system is smaller than R_{0i}, the output power of the full-bridge mode is higher than that of the half-bridge mode. Thus, switch S_1 is turned OFF to activate the full-bridge mode. On the other hand, when the dc load is larger than R_{0i}, the output power of the half-bridge mode is higher than that of the full-bridge mode. Then, S_1 is turned ON for the half-bridge mode operation. As a result, by switching between these two modes, we can achieve high output power over a wide load range.

D. Control Diagram

From the theoretical analysis, it can be seen that the FSMFEH system operating mode is selected by comparing the load resistance R_0 and R_{0i}. R_0 can be calculated by measuring the load voltage and current, and it is compared with R_{0i} to determine whether switch S_1 is switched. The switching procedure is shown in Fig. 8. If R_0 is smaller than R_{0i}, switch S_1 is turned OFF to activate the full-bridge mode. When R_0 is larger than R_{0i}, switch S_1 is turned ON to activate the half-bridge mode. The circuit diagram with mode switching is shown in Fig. 9.

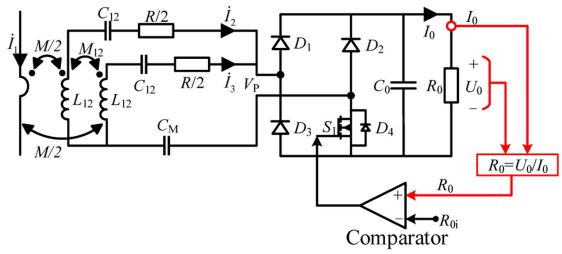

Fig. 9. Circuit diagram with mode switching.

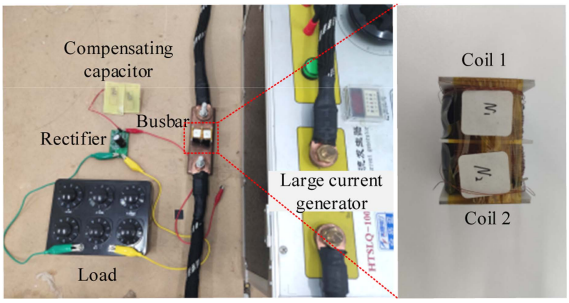

Fig. 10. Experimental platform.

TABLE I
PARAMETERS OF THE EXPERIMENT

Parameters	Value	Parameters	Value
Core material	Permalloy	Wire diameter	0.15 mm
f	50 Hz	I_1	100 A
N_1	3500	N_2	3500
R_1	224.4 Ω	R_2	229.9
L_1	1.3666 H	L_2	1.3319 H
C_1	36.1 μF	C_2	41.2 μF
M_{12}	1.08597 H	C_M	9.33 μF

IV. Experimental Verifications

A. Prototype Setup

To verify the analysis above, an experimental platform is built in the laboratory, as shown in Fig. 10. The large current generator outputs a 50 Hz ac to simulate the busbar current. The magnetic core consists of a 38 mm × 6 mm × 6 mm core and two 1 mm × 30 mm × 30 mm core laminations. The specific parameters of the experiment are given in Table I. Two coils are constructed in such a way that the parameters are as close as possible in manufacturing.

B. Experimental Results

The experimental curves of P against R_L under different modes are shown in Fig. 11. Its trend is consistent with the theoretical curves. The experimental waveforms of U_0, I_1, and V_P are shown in Fig. 12, and the root mean square of the busbar current is always 100 A.

When the load value is smaller than the R_{0i} value 300 Ω, the proposed FSMFEH is controlled to operate in the full-bridge mode because the output power of the full-bridge mode is higher than that of the half-bridge mode. The optimal load R_{F0_opt} and the maximum output power P_{FMAX} are 150 Ω and 11.2 mW, respectively. Then, once the load value is larger than the R_{0i} value 300 Ω, the proposed system is switched to the half-bridge mode. In this scenario, the optimal load R_{H0_opt} and the maximum output power P_{HMAX} become 600 Ω and 12 mW, respectively.

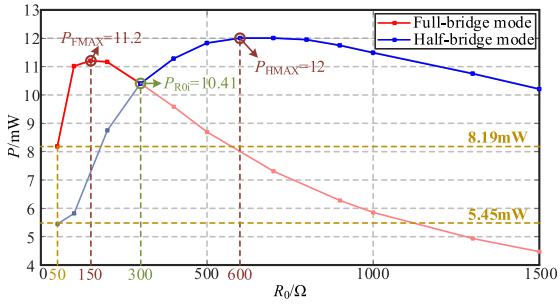

Fig. 11. Experimental curves that P against R_0 under the different modes.

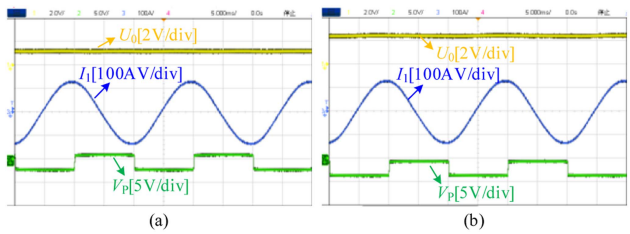

Fig. 12. Experimental waveforms. (a) Full-bridge mode, $R_{F0\_opt} = 150\ \Omega$. (b) Half-bridge mode, $R_{H0\_opt} = 600\ \Omega$.

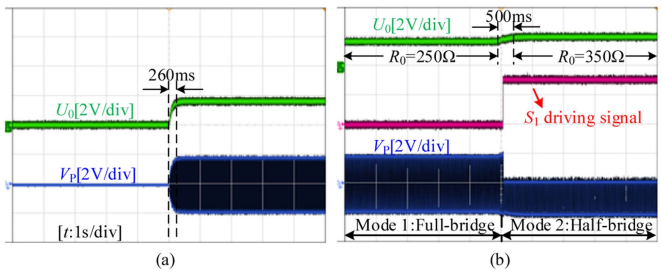

Fig. 13. Experimental results of the dynamic response. (a) When the system starts. (b) When the load changes.

According to the theoretical analysis, the output power of the conventional system is equal to the half-bridge mode of the proposed system. It can be seen from Fig.11, over the 50–1500 Ω load range, the output power increases from the output power limit of 5.45–12 mW of the conventional system to 8.19–12 mW in this letter. Especially, when $R_O = 100\ \Omega$, the output power of the proposed FSMFEH system can achive 11.025 mW, which is approximately 89.4% higher than the 5.82 mW output power of the conventional system.

C. Dynamic Transient

The dynamic response waveform of the proposed system is shown in Fig. 13. Fig. 13(a) shows the dynamic response of the system during start, and the startup time is about 260 ms. Besides, the system can start smoothly without impure or pulsating. The dynamic response of the system during load change is shown in Fig. 13(b). When the load changes from 250 to 350 Ω, the S_1 driver signal changes from a low level (0 V) to a high level (3.3 V), and the system working mode is switched

TABLE II
THE COMPARISON OF [10], [11], [12] AND THIS LETTER

	Core size (cm×cm×cm)	Cost	Complexity	The maximum output power(power density)	Output power range (load range)
[10]	15×10×10	high	medium	0.36 mW(1.86 μW/cm^3)	0.36 mW(Fixed in 6.03 kΩ)
[11]	15×10×10	high	high	0.612 mW(2.1 μW/cm^3)	0.612 mW(Fixed in 13.96 kΩ)
[12]	24.2×10×10	high	low	200 mW(0.668 mW/cm^3)	40–200mW(10–200 Ω)
This letter	4×3×3	low	low	12 mW(3.788 mW/cm^3)	8.19–12mW(50–1500 Ω)

from the full-bridge mode to the half-bridge mode. The response time of the system from the full-bridge mode to the half-bridge mode is about 500 ms. It can be seen from the waveform that the two modes can be switched smoothly.

D. Comparison and Discusssion

The comparison of [10], [11], [12] and this letter is given in Table II. Compared with [10], [11], [12], the proposed method in this letter can achieve power improvements over a wide range of loads with a smaller core size, lower cost and simpler core fabrication. Meanwhile, compared with [10], [11], [12], the proposed method has a better effect of maintaining high output power over a wide load range, that is, the proposed method can achieve a smaller output power change over a wider load range. Yuan et al. [10], [11] only show the effect of power improvement under fixed load, and the situation of power improvement under a wide range of load is not clear, but obviously they have a lower output power compared with this letter. In [12], over the 10–200 Ω load range, the maximum output power is 200 mW, the minimum output power is 40 mW, and the percentage of power decrease is 80%. In this letter, over the 50–1500 Ω load range, the maximum output power is 12 mW, the minimum output power is 8.19 mW, and the percentage of power decrease is only 31.75%. In conclusion, the proposed method in this letter can more effectively maintain high output power over a wide load range.

V. CONCLUSION

In this letter, a new FSMFEH system is proposed to maintain high output power over a wide load range. The novelty lies in the rectifier-based reconfigurable structure with two coils connected in parallel, leading to two operation modes. The equivalent ac load of the half-bridge mode is four times that of the full-bridge mode, but the maximum output power is kept the same. By switching between two modes properly according to the actual load demand, more power can be captured significantly. The experimental results show that the proposed FSMFEH system can harvest at least 8.19 mW of power under a load range from 50 to 1500 Ω when the busbar current is 100 A.

REFERENCES

[1] Y. Li, N. Duan, Z. Liu, J. Hu, and Z. He, "Impedance-matching-based maximum power tracking for magnetic field energy harvesters using active rectifiers," *IEEE Trans. Ind. Electron.*, to be published, doi: 10.1109/TIE.2022.3219064.
[2] R. Moghe, A. R. Iyer, F. C. Lambert, and D. M. Divan, "A low-cost wireless voltage sensor for monitoring MV/HV utility assets," *IEEE Trans. Smart Grid*, vol. 5, no. 4, pp. 2002–2009, Jul. 2014.
[3] S. K. Wankhede, P. Paliwal, and M. K. Kirar, "Bi-level multi-objective planning model of Solar PV-battery storage-based ders in smart grid distribution system," *IEEE Access*, vol. 10, pp. 14897–14913, 2022.
[4] Z. Zhang, M. Zhou, Z. Wu, S. Liu, Z. Guo, and G. Li, "A frequency security constrained scheduling approach considering wind farm providing frequency support and reserve," *IEEE Trans. Sustain. Energy*, vol. 13, no. 2, pp. 1086–1100, Apr. 2022.
[5] Y. Li, C. Zhou, X. Wang, J. Wang, D. Qiao, and K. Tao, "A vibration energy harvester with targeted frequency-tuning capability," *IEEE Trans. Instrum. Meas.*, vol. 71, pp. 1–10, May 2022, Art. no. 7503010.
[6] Z. Liang and J. Yuan, "A compact dual-band four-port ambient rf energy harvester with high-sensitivity, high-efficiency, and wide power range," *IEEE Trans. Microw. Theory Techn.*, vol. 70, no. 1, pp. 641–649, Jan. 2022.
[7] Z. Liu, Y. Li, H. Yang, N. Duan, and Z. He, "An accurate model of magnetic energy harvester in the saturated region for harvesting maximum power: Analysis, design, and experimental verification," *IEEE Trans. Ind. Electron.*, vol. 70, no. 1, pp. 276–285, Jan. 2023.
[8] F. Yang and L. Du and H. Yu, and P. Huang, "Magnetic and electric energy harvesting technologies in power grids: A review," *Sensors*, vol. 20, no. 5, 2020.
[9] N. M. Roscoe and M. D. Judd, "Harvesting energy from magnetic fields to power condition monitoring sensors," *IEEE Sensors J.*, vol. 13, no. 6, pp. 2263–2270, Jun. 2013.
[10] S. Yuan, Y. Huang, J. Zhou, Q. Xu, C. Song, and P. Thompson, "Magnetic field energy harvesting under overhead power lines," *IEEE Trans. Power Electron.*, vol. 30, no. 11, pp. 6191–6202, Nov. 2015.
[11] S. Yuan, Y. Huang, J. Zhou, Q. Xu, C. Song, and G. Yuan, "A high-efficiency helical core for magnetic field energy harvesting," *IEEE Trans. Power Electron.*, vol. 32, no. 7, pp. 5365–5376, Jul. 2017.
[12] K. Yang et al., "Magnetic field energy harvesting from the traction return current in rail tracks," *Appl. Energy*, vol. 292, 2021, Art. no. 116911.
[13] H. Yang, Y. Li, Z. Liu, H. Luo, Y. Yan, and Z. He, "An accurate power model and high power density design method of free-standing magnetic field energy harvesters with h-shaped core," *IEEE Trans. Ind. Electron.*, to be published, doi: 10.1109/TIE.2022.3225854.
[14] S. Arslan and S. A. A. Shah, and H. Kim, "An ultra-wide load range voltage converter using proactive phase frequency modulation for iot sensors," *Sensors*, vol. 20, no. 21, pp. 1–13, 2020.
[15] R. Mai, Y. Liu, Y. Li, P. Yue, G. Cao, and Z. He, "An active-rectifier-based maximum efficiency tracking method using an additional measurement coil for wireless power transfer," *IEEE Trans. Power Electron.*, vol. 33, no. 1, pp. 716–728, Jan. 2018.